J Mater Sci (2011) 46:6863–6870
DOI 10.1007/s10853-011-5649-7

The mechanical response of Rohacell foams at different length scales

S. Arezoo · V. L. Tagarielli · N. Petrinic · J. M. Reed

Received: 19 March 2011 / Accepted: 19 May 2011 / Published online: 8 June 2011

Abstract The quasi-static mechanical response of polymethacrylimide (PMI) foams of density ranging from 50 to 200 kg m^{-3} is investigated in order to provide experimental data to inspire and validate numerical constitutive models for the response of polymer foams. The macroscopic mechanical response is characterised by conducting quasi-static compression, tension, shear and indentation experiments, whereas microscopic deformation mechanisms are identified by conducting in situ SEM observations during static compression and tension tests; it is shown that foams of low density collapse by cell wall buckling while foams of high density undergo plastic cell-wall bending. As a result, both the elastic and plastic macroscopic response of the foam display a tension/compression asymmetry.

Introduction

Polymeric foams are plastically compressible solids widely used as a core material in structural sandwich components due to their low density and high energy absorption. Other applications of foams include sports products, packaging, transport, as well as automotive and aerospace components.

Several authors have investigated the compressive response of cellular solids at low and high rates of strain [1–8]. Others [9, 10] have developed micro-mechanical models in order to predict the material response to different loading cases, relating it to the properties of the parent material, to the cell topology and to the relative density.

Rohacell is the trade-name for a closed-cell, rigid foam made from polymethacrylimide (PMI), which can be produced in different grades and densities. In this study, we shall explore the response of Rohacell Grade WF; this class of foams retains reasonably good mechanical properties at high temperature and for this reason is considered as a potential core material for advanced sandwich components operating at relatively high temperatures.

The mechanical properties of Rohacell WF have been investigated by several researchers. Li and Mines [11] performed uniaxial and hydrostatic compression, tension and shear tests on Rohacell 51WF (density $\rho = 51\,\mathrm{kg\,m^{-3}}$). Results from their experiments were in good agreement with the analytical predictions by Chen et al. [10] for this particular foam density.

Benderley et al. [12] investigated the shear strength of Rohacell 200WF (density $\rho = 200\,\mathrm{kg\,m^{-3}}$) by testing a sandwich beam in four-point bending and subjecting the material to a combination of shear and compressive stresses; they found that the maximum shear stress and compressive stress at failure were related by a quadratic law.

Zenkert et al. [13] reported uniaxial compression and tension experiments on three densities of Rohacell WF foams ($\rho = 51,\ 110,\ 200\,\mathrm{kg\,m^{-3}}$). Their results showed that for foams of low density the compressive strength was lower than the tensile strength; the opposite was found for foams of higher density. They argued that this was due to the occurrence of elastic buckling of the cell walls for the low-density foams, but provided no supporting evidence for this.

Flores-Johnson et al. [14] investigated the degradation of compressive foam stiffness of Rohacell 51WF ($\rho = 51\,\mathrm{kg\,m^{-3}}$) with increasing compressive plastic strain.

S. Arezoo · V. L. Tagarielli (✉) · N. Petrinic
Engineering Department, University of Oxford, Parks Road, Oxford OX1 3PJ, UK
e-mail: vito.tagarielli@eng.ox.ac.uk

S. Arezoo · J. M. Reed
Rolls-Royce plc, PO Box 31, Derby DE24 8BJ, UK

Zenkert et al. [15] used data from a uniaxial compression test on Rohacell 51WF to calibrate Finite Element (FE) constitutive models, in order to predict the indentation response of composite sandwich plates; predictions were accurate up to the occurrence of brittle fracture within the core material. Similarly, other authors performed three point bending [16] and indentation tests [17] on sandwich panels with polymer foam cores and modelled these experiments via FE simulations.

In this article, we present results from quasi-static experiments conducted on four different densities of Rohacell WF ($\rho = 51,\ 71,\ 110,\ 200\,\mathrm{kg\,m^{-3}}$). The stress versus strain responses of the different foams are measured in uniaxial compression and tension as well as in shear and indentation. In situ compression and tension experiments are conducted to explore the mechanisms of deformation of foams of different densities.

We begin by describing experimental techniques and presenting experimental results, we then proceed to discuss the results, attempting to establish a connection between the observed microscopic mechanisms and the measured macroscopic mechanical response of the foams.

Experimental investigation

Material

Polymethacrylimide or "Rohacell" WF foams [18] are made from a copolymer of methacrylonitrile (C_4H_5N) and methacrylic acid ($C_4H_6O_2$), with a few key additives and including alcohol as a foaming agent. A ductile thermoset polymer is chemically formed and solidified, and subsequently foamed by thermal expansion of the polymer sheet in large ovens and at high temperatures.

The material examined in this study was obtained in the form of large, 50 mm thick plates of four different densities, namely 51, 71, 110 and 200 kg m^{-3}; these four materials will be denoted by R51, R71, R100 and R200, respectively. The relative density of each foam was calculated as the ratio of the measured foam density to the density of the parent polymer (obtained from manufacturer data sheets as 1416 kg m^{-3}); Table 1 presents results from these measurements.

An environmental scanning electron microscope (ESEM) was employed to observe the details of the foams microstructure. Figure 1 shows four micrographs for the four foam densities investigated here. The shape of the closed cells was similar to the idealised tetrakaidecahedral geometry, as recognised by other authors [9, 10]. For this foam geometry, Gibson and Ashby [9] have provided predictive formulae to obtain the relative density as a function of geometrical parameters. The average cell size, cell-wall length and thickness were measured from statistical analysis of the ESEM scans and results from these measurements are presented in Table 1, which includes values of the slenderness ratio of the cell walls, as well as the measured and predicted relative densities. The predictions from Gibson and Ashby [9] are accurate for low density foams, but they under-predict the relative density of foams of a higher density.

Uniaxial compression experiments

Uniaxial compression tests were conducted at room temperature on cuboidal specimens measuring 20 × 20 × 10 mm. The specimens were loaded at a nominal strain rate of 0.01 s^{-1} by flat platens, lubricated with a PTFE spray. The load was applied by a screw-driven machine and measured with a resistive load cell. Compressive strains were measured by a non-contact laser extensometer of resolution 1 μm and gauge length equal to the specimen height.

Preliminary checks revealed that the compressive material response was isotropic. All tests were replicated five times on identical specimens and the measured stress versus strain responses were highly repeatable, with scatter below 5%. Typical stress–strain compressive responses for all four foam densities are shown in Fig. 2. The foam response comprised a linear phase followed by a stress plateau characterised by negligible strain-hardening, and final densification. Negligible lateral strain was observed, implying that for these foams the plastic Poisson's ratio is close to zero.

Table 1 Measured average micro-structural parameters for the four foams under investigation, and predicted relative density according to Gibson and Ashby [9]

Density (kg m^{-3})	Cell diameter (μm)	Edge length (μm)	Edge thickness (μm)	Cell wall slenderness ratio	Measured relative density	Predicted relative density
51	380	230	7	35.54	0.036	0.033
71	960	510	17	29.61	0.053	0.040
110	930	580	14	39.85	0.078	0.030
200	640	350	28	12.36	0.142	0.096

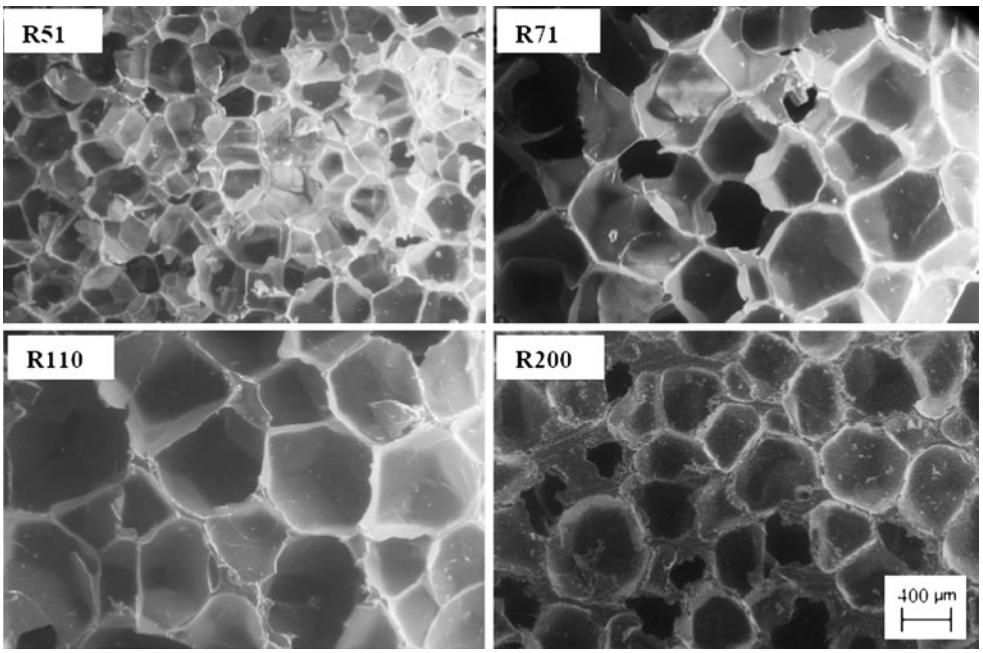

Fig. 1 ESEM micrographs of the four foams investigated in this study, showing the variation of material microstructure with relative density

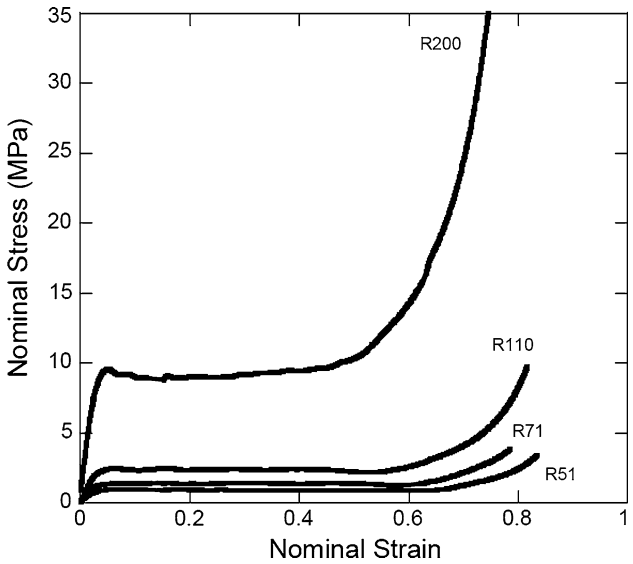

Fig. 2 Quasi-static nominal compressive stress–strain response of the four foam densities, at a strain rate of 0.01 s^{-1}

Measured mechanical properties are reported in Table 2 for all foam densities. The compressive Young's modulus was measured upon elastic unloading at a plastic compressive strain of ~ 0.05, in order to obtain measurements independent of specimen surface finish or slight misalignment of the compression platens. The table includes values of the measured compressive plateau stress σ_{PL}, compressive yield stress σ_{Yc} (defined as the flow stress at a nominal plastic strain of 0.2%) and densification strain ε_D (defined as the nominal compressive strain at a flow stress of $2\sigma_{PL}$).

Uniaxial tension experiments

Uniaxial tensile tests were carried out on flat dogbone specimens with a gauge portion measuring $9 \times 4 \times 36$ mm. The tensile force was applied through aluminium end-caps bonded to the specimen's ends; the end-caps were connected to the test machine by a pin-joint in order to eliminate spurious bending moments.

Table 2 Measured quasi-static mechanical properties of the four foam densities under investigation. Measured scatter was below 5% on all properties

	E_c (MPa)	E_t (MPa)	G (MPa)	σ_{Yc} (MPa)	σ_{PL} (MPa)	ε_D	σ_{Yt} (MPa)	σ_{Ft} (MPa)	τ_Y (MPa)	τ_F (MPa)
Roh51	32.5	74	15.3	0.95	0.93	0.77	1.2	1.44	0.53	0.75
Roh71	48.5	101.5	28.8	1.39	1.39	0.75	1.64	1.75	0.77	1.04
Roh110	82.5	128	40.6	2.48	2.36	0.73	2.05	2.17	1.29	1.86
Roh200	246.5	385	164	9.6	9.1	0.65	5.7	7.71	3.57	4.94

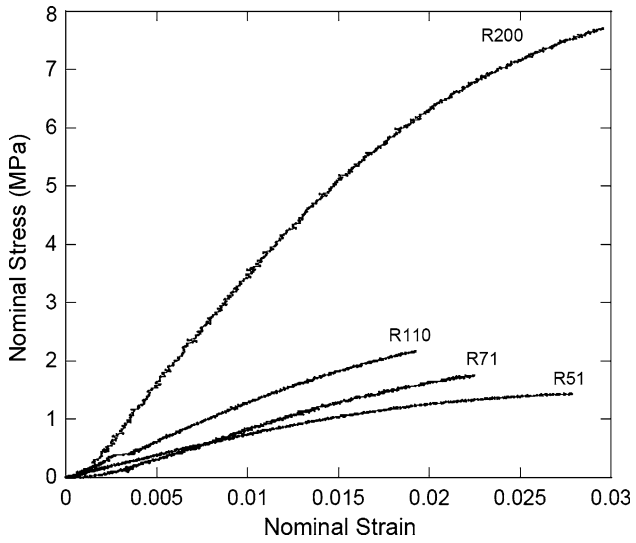

Fig. 3 Tensile nominal stress–strain response of the four foam densities under investigation, at a strain rate of 0.01 s^{-1}

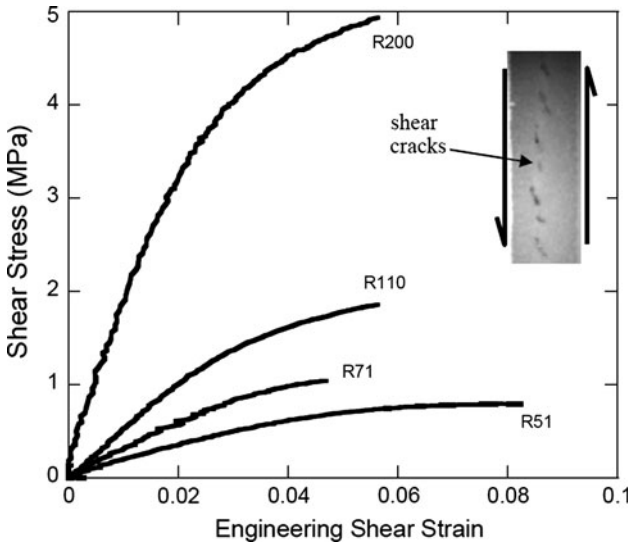

Fig. 4 Measured engineering shear stress versus strain response of the Rohacell foams at an engineering shear strain rate of 0.01 s^{-1}

Tests were again conducted at a nominal strain rate of 0.01 s^{-1}. The load was measured by a resistive load cell, while strains were measured by a non-contact laser extensometer with gauge length of 5 mm. The stress versus strain response for the four foams is presented in Fig. 3. For all densities, the response comprised an initial linear elastic phase followed by a non-linear phase of pronounced strain-hardening.

Brittle failure occurred at nominal strains of 2–3% by the propagation of a crack perpendicular to the loading direction. Table 2 includes the measured tensile elastic modulus, tensile failure stress σ_{Ft} and tensile yield stress σ_{Yt} for all foams; again, the yield stress in tension is defined as the tensile flow stress at a plastic nominal strain of 0.2%.

Shear experiments

Single-lap shear experiments were conducted using prismatic foam specimens with an I-shaped cross-section, with shear deformation occurring only in the web of the I-beam. This specimen geometry was preferred to a prismatic beam of rectangular cross-section as an I-shaped cross-section allows reduction of stresses at the interface between the foam and the metallic fixture used to load it, reducing the risk of premature specimen failing by delamination.

The web of the I-shaped cross-section, representing the gauge section of the specimen, had a height of 10 mm and a width of 6 mm, whereas the depth was 120 mm to ensure a high depth to height ratio, in order to minimise edge effects. The thickness and width of the I-beam flanges was of 6 and 30 mm, respectively. The web was connected to foam flanges by fillets of radius 2 mm.

The I-beam was sandwiched between two steel plates and bonded to these by a structural adhesive; the plates were connected to a screw-driven test machine by pin-joints. During the experiment, the test machine reduced the spacing between the pin-joints, therefore applying a compressive force on the steel fixture, resulting in a shear action on the I-shaped foam core. A non-contact laser extensometer of resolution 1 μm and gauge length 10 mm was employed to record the relative displacement between the two flanges of the I-beam, thereby determining the engineering shear strain.

The measured stress/strain responses in shear for the four foams are reported in Fig. 4. They comprise a linear elastic regime, followed by a nonlinear phase. Failure was by formation of shear micro-cracks in the central portion of the web, as seen in the insert of Fig. 4. Table 2 lists values for the shear modulus G, the stress at failure τ_F and the shear yield stress τ_Y (defined as the shear flow stress at a plastic engineering shear strain of 0.2%) for the four foam densities. The measured values were in line with those reported by material data-sheets [18] and in existing literature [13].

Indentation experiments

In order to explore the response of the foams to a multi-axial state of stress, indentation tests were performed using a spherical steel indenter of radius 12.5 mm. The indenter was displaced at constant speed to indent cuboidal blocks of foams of dimensions 120 × 120 × 50 mm; the maximum indentation depth was set to 10 mm in order to eliminate specimen boundary effects. The indentation speed was chosen to give an average representative strain

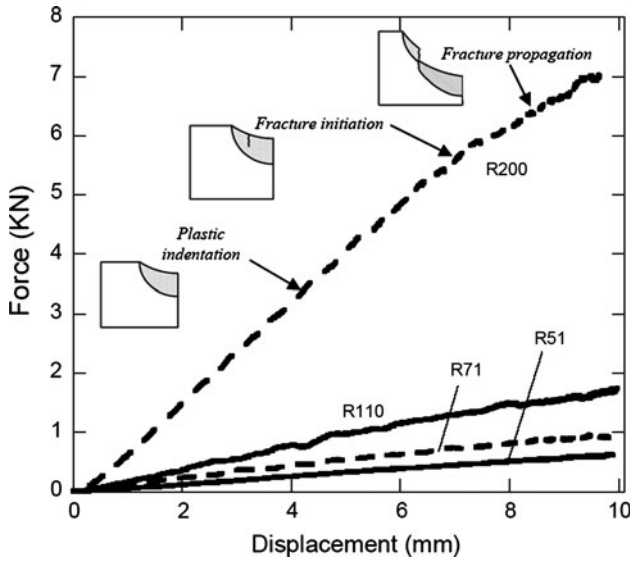

Fig. 5 Measured indentation force versus displacement response for the four foam densities

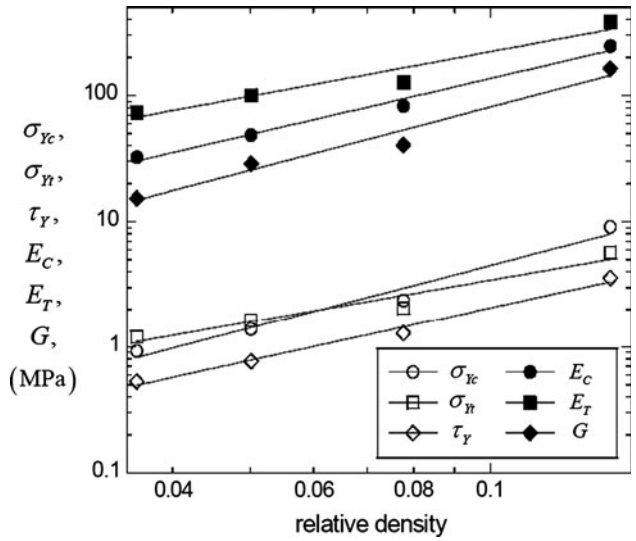

Fig. 6 Scaling of elastic and plastic properties with the relative density of the foam. Average values are reported; the data scatter was less than 5% on all properties. Scaling of elastic and plastic properties with the relative density of the foam

rate of 0.01 s^{-1} at an indentation depth of 5 mm (a representative strain rate in an indentation test can be taken as $\dot{\varepsilon} = \dot{h}/h$, where h is the indentation depth and the dot denotes differentiation with respect to time).

The measured indentation force versus displacement curves are presented in Fig. 5; load increased in a nearly linear manner with displacement, up to an indentation depth of $\sim$7 mm; in this phase deformation proceeded by plastic indentation of the foam beneath the indenter, as revealed from results of interrupted tests. At 7 mm indentation depth, brittle cracking of the foam occurred for all densities, and the ensuing load/displacement response became non-linear. Observations subsequent to the tests confirmed that a cylindrical crack had formed under the indenter and had propagated in the loading direction, as shown in the inserts of Fig. 5 for a R200 foam. For all foam densities, the indentation response was characterised by negligible pile-up or sink-in; this is expected for plastically compressible solids [19].

In situ compression and tension experiments

Figure 6 summarises the dependence of some stiffness and strength parameters of Rohacell foams upon the foams relative density (the power-law fits through the experimental data shown in Fig. 6 gave the intercepts and exponents listed in Table 3). The figure shows that the yield stress is higher in tension than in compression for low-density foams, whereas the opposite is seen for high-density foams. This is in line with the findings of Zenkert et al. [14], who justified this by conjecturing that elastic buckling mechanisms might intervene in the compressive deformation of low-density foams,

Table 3 Intercepts (A) and exponents (b) for power-law fits of the experimental data shown in Fig. 6

$Y = A\bar{\rho}^b$	A (MPa)	b
σ_{Yc}	105	1.66
σ_{Yt}	44	1.11
τ_Y	51	1.39
E_C	4106	1.47
E_T	3333	1.17
G	3784	1.66

reducing the measured yield stress. The measured elastic response of the foam is asymmetric, with the material tensile modulus greater than the compressive modulus, especially for foams of low density.

Several micromechanical models for the response of an idealised foam geometry [9, 10] predict equal stiffness and yield stresses in tension and compression, based on the assumption that the collapse in both uniaxial tension and compression is governed by a plastic cell-wall bending mechanism. On the other hand some authors [20] have recognised that low-density foams with slender cell-walls can collapse under a macroscopic compressive stress by elastic buckling of the cell-walls.

In order to explore the differences in the compressive deformation mechanisms between low- and high-density foams, in situ compression tests were performed in the ESEM. A loading stage of capacity 5 kN was employed to compress cubic specimens of 5 mm side between two flat, lubricated plates. Test specimens were cut using a diamond-grit miniature disk saw which minimised surface

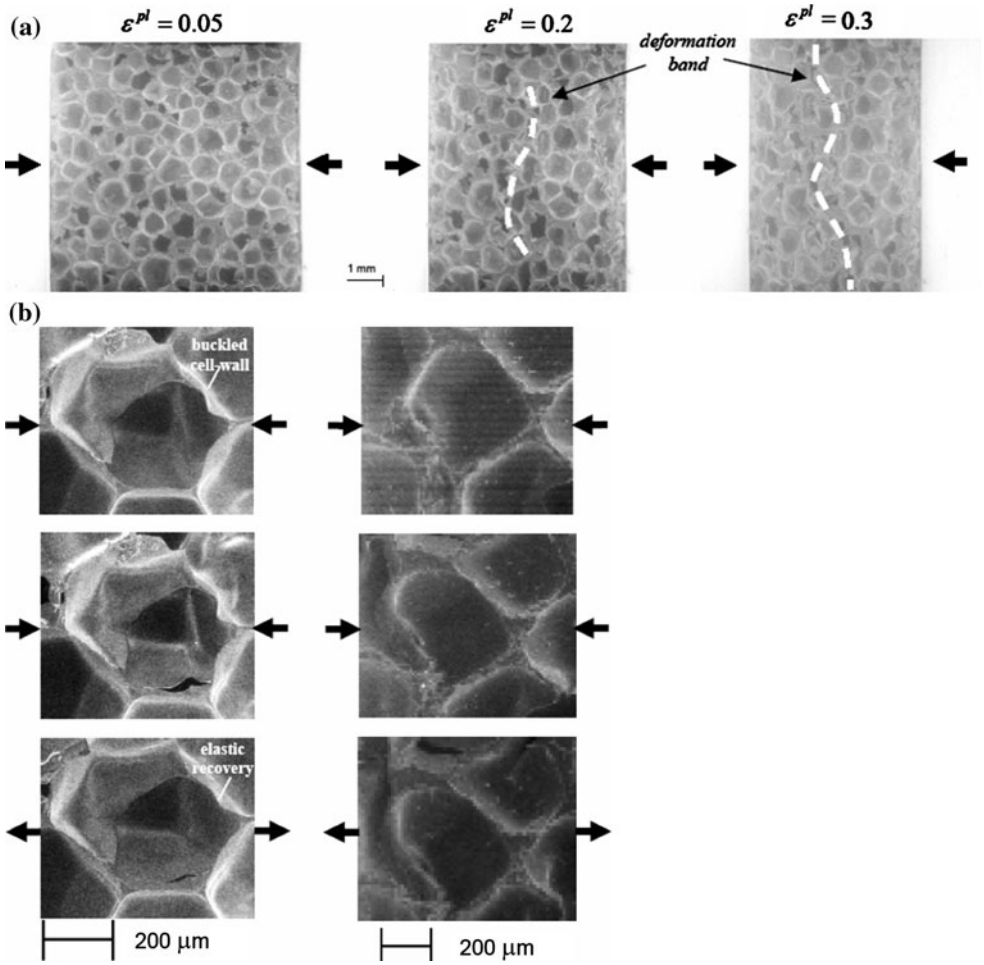

Fig. 7 **a** ESEM scans from an in situ compression test on the R200 foam; uniform plastic deformation is followed by strain localisation, initiated by plastic bending of the cell walls. **b** *Left* ESEM scans from an in situ compression test on the R51 foam, showing cell wall buckling followed by elastic unloading. *Right* Similar ESEM scans for foam R200, showing cell wall plastic bending, with permanent deformation upon unloading

damage to the specimens. The tests were occasionally interrupted in order to take ESEM scans, which were also processed in order to measure the macroscopic compressive strain.

The in situ compression tests revealed that plastic deformation of the foam was initially uniform, up to plastic compressive strains of the order of 5%. Beyond this strain level, premature collapse of individual cells triggered localisation of deformation along bands perpendicular to the loading direction and of width of the order of the cell size. Such bands increased their length and thickness with continued macroscopic compressive deformation, as is shown in Fig. 7a for a R200 specimen. Some specimens collapsed by formation of multiple deformation bands and their final coalescence.

The mechanism by which individual cells collapse was found to depend on foam density. The left-hand side of Fig. 7b shows a sequence of three ESEM scans of a R51 foam undergoing compression, in displacement control; the first frame shows the initiation of elastic buckling of an initially straight cell-wall upon compressive loading. As the load is increased further, the lateral deflection of the buckled edge increases and a crack develops in an adjacent cell-wall. The sample is then unloaded and the buckling deformation is partially recovered.

The right-hand side of Fig. 7b shows the deformation of a R200 foam cell consequent to a similar loading–unloading sequence. This thick-walled cell initially deforms by bending of the cell wall upon loading; subsequent unloading revealed that this deformation was permanent, and therefore plastic bending had taken place.

The in situ compression tests described above showed that foams of low density collapsed by a combination of elastic buckling and plastic bending, with slender cell walls undergoing elastic buckling and stockier cell walls experiencing plastic bending. In high-density foams, the thick-walled cells deformed primarily by plastic bending of cell walls. Some tensile tests conducted in the ESEM revealed that the microscopic deformation mechanism was similar for high- and low-density foams; this consisted of bending and stretching of the foam cell walls, while failure was by fast propagation of a fast unstable crack.

In situ compression tests revealed that elastic cell-wall buckling occurred in the low-density foams even at very low levels of applied stress; typically, this was observed in cells of large diameter and with slender cell-walls. The existence of this mechanism may justify the measured asymmetry of the elastic moduli in tension and compression; this asymmetry is indeed more pronounced in foams of low relative density.

Concluding discussion

Analysis of the microstructure of the four foams under investigation revealed that the material comprises cells of tetrakaidecahedral shape, with different cell diameter and cell-wall thickness for each foam density; no simple scaling laws could be identified relating geometrical microstructural features to the foam relative density: the foam microstructure is strongly dependent on the manufacturing process (as well as on relative density). Cell diameter, cell-wall slenderness and their statistical distributions can deeply affect the macroscopic foam response; for example, foams R110, of relatively high density, possess the highest average cell wall slenderness (39) of all foams investigated. The data presented in Fig. 6 suggests that the measured stiffness and strength parameters of the R110 foam are systematically lower than the values predicted by the power-law fits $Y = A\bar{\rho}^b$ (Table 3). It appears reasonable to argue that this is due to the high slenderness of the R110 cell-walls, promoting elastic buckling mechanisms.

Foams of lower relative density and slender cell-walls display a tendency to undergo elastic buckling of the cell-walls under macroscopic compressive loading, while this phenomenon is not observed for foams of higher density and thicker cell-walls. The tendency of the low-density foams towards elastic cell wall buckling in compression is observed even at low levels of stress, corresponding to the initial linear macroscopic response of the material. This observation is consistent with the measured asymmetry of elastic moduli in tension and compression, for a given foam density.

In situ experiments revealed that macroscopic plastic collapse of the foams is driven by different mechanisms for low-density and high-density foams; collapse is initiated by a combination of elastic buckling and plastic bending of the cell walls for low-density foams, while plastic cell-wall bending is responsible for the macroscopic plastic collapse of high-density foams.

Existing micromechanical models for the elastic response of open-cell cellular solids (see for example [10]) predict that the material stiffness scales with the relative density according to a power-law. If the active deformation mechanism is driven by axial loading of the cell-wall (e.g. cell-wall buckling), these models predict a power-law exponent approaching 1; on the other hand, if deformation is by cell-wall bending, the power-law exponent is 2 (for open-cell foams; the numerical values of the exponents of these scaling laws are slightly reduced for the case of closed-cell foams). The data presented in Fig. 6 suggests that the measured variation of compressive elastic modulus with $\bar{\rho}$ could be better fitted by two distinct power-law expressions: namely, a power-law of exponent around 1.2 for $\bar{\rho} < 0.08$, and a power-law of exponent 1.8 for $\bar{\rho} > 0.08$. The observed increase in power-law exponent with relative density is consistent with the notion of different deformation mechanisms active for the low-density and high-density foams.

The measured indentation response and microscope observation of the indentation specimens revealed that fracture occurs at similar indentation depths (and therefore at similar strains) in all foams investigated, and that cracks initiate in the region of densified foam under the indenter. Here, foams have acquired a locally anisotropic response due to strain-induced changes in their microstructure.

The experimental findings reported in this study suggest that the geometric features of the foam microstructure and their statistical distribution can substantially affect the macroscopic mechanical response. The tension/compression asymmetry of foam stiffness and yield stress are examples of the effect of foam microstructure on its macroscopic response. Such effects can be captured by existing continuum, phenomenological numerical models and associated (lengthy) multi-axial calibration experiments (see for example [20]); however, such models are unable to capture strain-induced anisotropy and the details of brittle foam fracture in the presence of tensile principal stresses. A physically based, multi-scale modelling approach incorporating stochastic aspects of the foam microstructure, can in principle provide detailed predictions of all aspects of the mechanical response of foams; the development of this modelling approach is left as a topic for a future study.

Acknowledgements The authors would like to thank Rolls-Royce plc for the provision of financial support for Sara Arezoo's PhD project. We are grateful to Röhm Ltd for providing the Rohacell foams and acknowledge the assistance of Mr P. Siegkas with experiments.

References

1. Subhash G, Liu Q, Gao X (2005) Int J Impact Eng 329:1113
2. Eaves D (2004) Handbook of polymer foams, vol 1. Rapra Technology Limited, Shropshire, p 290
3. Song B, Chen W, Lu W-Y (2007) J Mater Sci 42(17):7502. doi: 10.1007/s10853-007-1612-z
4. Mills N (2007) Polymer foams handbook: engineering and biomechanics applications and design guide. Elsevier Ltd, Amsterdam, p 535

5. Mines RAW (2008) Strain 44:71
6. Reid SR, Peng C (1997) Int J Impact Eng 19:531
7. Tagarielli VL, Deshpande VS, Fleck NA (2007) Compos B 39:83
8. Deshpande VS, Fleck NA (2000) Int J Impact Eng 24(3):277
9. Gibson LJ, Ashby MF (1999) Cellular solids: structure and properties, 2nd edn. Cambridge University Press, Cambridge, p 532
10. Chen CP, Lakes RS (1995) Cell Polym 14:186
11. Li QM, Mines RAW, Birch RS (1999) Int J Solids Struct 37(2000):19
12. Benderly D, Putter S (2004) J Polym Test 23:51
13. Zenkert D, Burman M (2009) Compos Sci Technol 69:785
14. Flores-Johnson EA, Li QM, Mines RAW (2008) J Cell Plast 44(5):415
15. Zenkert D, Shipsha A, Persson K (2004) J Compos B 35(6–8):511
16. Steeves CA, Fleck NA (2004) Int J Mech Sci 46:585
17. Rizov V, Shipsha A, Zenkert D (2005) J Compos Struct 69(1):95
18. Roehm (1998) Rohacell WF PMI Foam. Roehm Ltd., Milton Keynes
19. Fleck NA, Otoyo H, Needleman A (1992) Int J Solids Struct 29:1613
20. Deshpande VS, Fleck NA (2001) Acta Mater 49(10):1859